Efficient design of small permanent magnet excited motors for automotive applications

Kay Hameyer & François Henrotte
Katholieke Universiteit Leuven, E.E. Dept. ESAT / ELECTA
Kasteelpark Arenberg 10, B-3001 Leuven-Heverlee
E-mail: Kay.Hameyer@esat.kuleuven.ac.be

***Abstract* – An increasing number of board-net components in nowadays cars can be stated. To satisfy the request of such high quality electro-mechanical devices, it is very important to have efficient design tools.**

Novel soft- and hard-magnetic materials offer the possibility for further miniaturisation and therefore the design of very compact new designs with a high energy density. To evaluate and study the various materials at all possible operating conditions appropriate models and their simulation are required.

In this paper the analytical design procedure, a very quick and efficient approach for standard auxiliary motors equipped with permanent magnet material for automotive applications is shown. For the design of special motors with particular properties an analytical design approach is not well suited and the finite element method can be employed to support the design engineer.

I. Introduction

Due to safety and luxury reasons for nowadays cars an increasing number of board-net components can be found (Fig. 1). In luxury cars more then a 100 small electric motors are installed to serve for various applications.

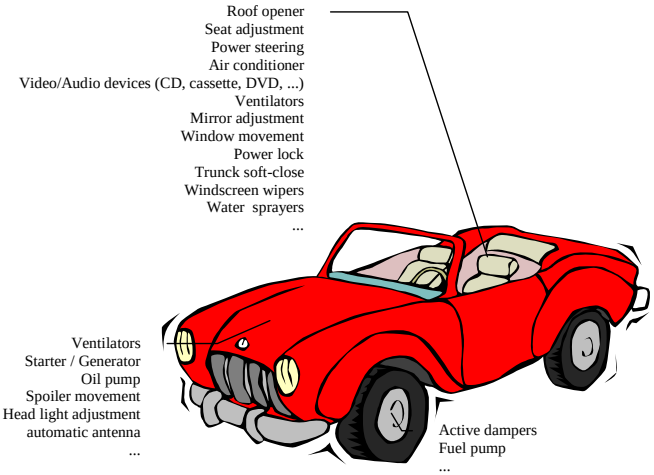

Fig. 1. Some examples of auxiliary motors and actuators in a nowadays car.

One of the aims for the design of such auxiliary motors is to optimise the motors objective to minimise its volume and weight. With the weight reduction an overall fuel-efficient car can be realised. As a consequence modern motor designs are very often equipped with novel hard-magnetic materials, such as high-energy permanent magnets based on rare earth components.

By minimising the overall volume of the motor and by simultaneously applying high-energy permanent magnet material particular attention has to be paid regarding saturation effects in the magnetic circuit. In such cases finite element models are very well suited for the design. To realise cost-effective dynamic models operated by power electronic circuits a combination of analytical and numerical model can be chosen. In this paper this efficient approach will be illustrated at an example of a permanent magnet excited brushless DC motor.

However, standard brushed automobile auxiliary motors are still equipped with ferrite permanent magnet material and therefore are not too much saturated. They can be analysed by analytical methods. To illustrate the effectiveness of both approaches, their strength and short-comings the analytical and the numerical one are briefly discussed and some examples of are given.

II. Quick Analytical Design

In the following section the basic equations of a small brushed DC motor (Fig. 2) will be discussed with respect to its design.

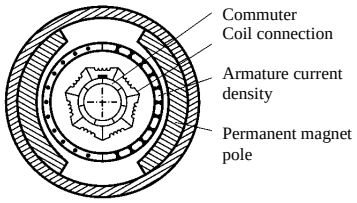

Fig. 2. Cross section of a brushed DC motor.

The induced voltage of the motor can be determined by:

$$U_{iL_A} = \int_{L_A} (\vec{v} \times B_L) d\vec{s} \quad , \tag{1}$$

the rotor's speed respectively pole pitch can be calculated by employing:

$$v = 2\pi \frac{D_A}{2} \cdot n \quad ; \quad \tau_p = \frac{\pi D_A}{2p} \quad . \tag{2}$$

This yields the induced voltage in one armature conductor (Fig. 3):

$$U_{iL_A} = vB_L l_A = 2p \cdot \tau_p n B_L l_A \tag{3}$$

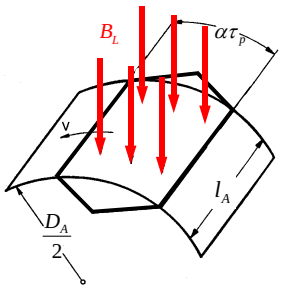

Fig. 3. Armature conductor and air gap field.

The winding consist of $z/2a$ conductors from which $\alpha \cdot \left(\frac{z}{2a}\right)$ are in the exciting field B_L. The flux per pole is then determined by:

$$\phi = \alpha \cdot \tau_p \cdot l_A \cdot B_L \tag{4}$$

and the induced voltage of the armature winding is finally:

$$U_i = \frac{z}{a} p \cdot \phi \cdot n \tag{5}$$

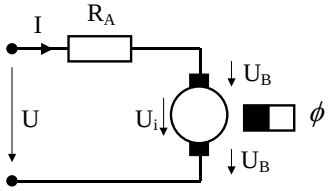

Fig. 4. Equivalent circuit of the brushed permanent magnet excited DC motor.

Determining the energy balance via the voltage equation:

$$\begin{aligned} I \cdot (U - 2U_B) &= I \cdot U_i + I^2 \cdot R_A \\ P_{el} &= P_{mech} + P_{lA} \\ &= M \cdot 2\pi n + P_{lA} \end{aligned} \tag{6}$$

yields the equation for the torque, respectively the speed characteristic depending on the pole-flux of the machine:

$$M \cdot 2\pi n = U_i \cdot I = \frac{z}{a} p \cdot \phi \cdot I \quad , \tag{7}$$

$$n = \frac{(U - 2U_B)}{\frac{z}{a} p \cdot \phi} - M \cdot \frac{2\pi \cdot R_A}{\left(\frac{z}{a} p \cdot \phi\right)^2} \tag{8}$$

Modifying eq. (7) yields the current:

$$I = \frac{2\pi}{\frac{z}{a} p \cdot \phi} \cdot M \tag{9}$$

Plotting now the functions:

$$\begin{aligned} M &= f\left(\frac{z}{a} p \cdot \phi\right) \\ &= \frac{(U - 2U_B)\left(\frac{z}{a} p \cdot \phi\right)}{2\pi \cdot R_A} - n \cdot \frac{\left(\frac{z}{a} p \cdot \phi\right)^2}{2\pi \cdot R_A} \end{aligned} \tag{10}$$

and

$$\begin{aligned} I &= f\left(\frac{z}{a} p \cdot \phi\right) \\ &= \frac{(U - 2U_B)}{R_A} - n \cdot \frac{\left(\frac{z}{a} p \cdot \phi\right)}{R_A} \end{aligned} \tag{11}$$

for a constant value of $U\text{-}2U_B$ and the speed n as parameter yields the graphs, which are used to design and optimise the motor (Figs. 5 & 6).

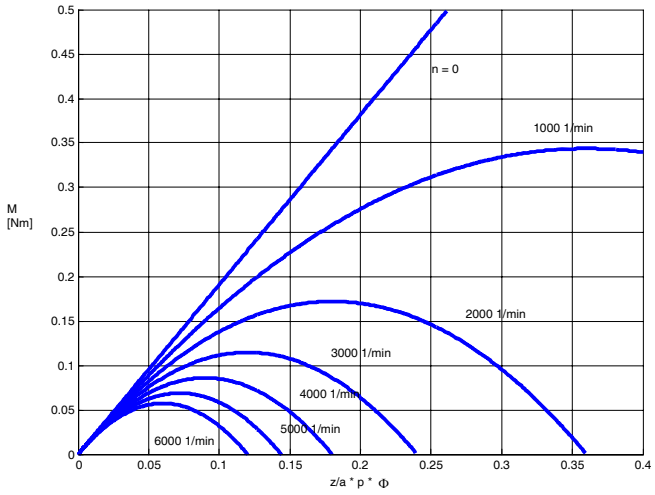

Fig. 5. Torque characteristics with parameter speed n.

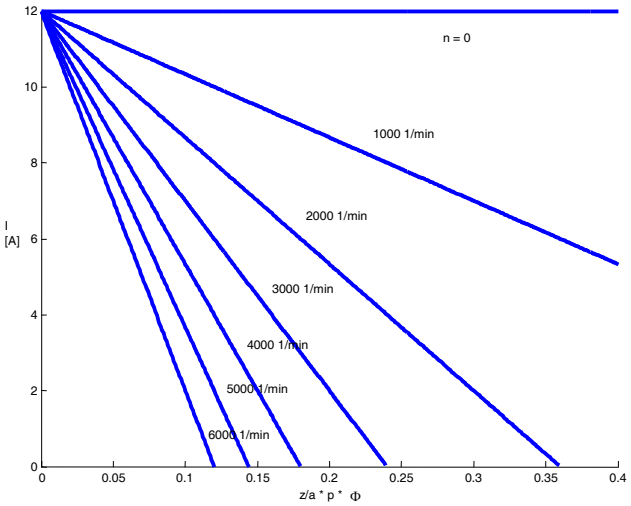

Fig. 6. Current characteristics with parameter speed n.

For the design of the motor the speed, as well depending on the pole flux can be drawn with (Fig. 7):

$$n = \frac{U - 2U_B}{\frac{z}{a} p \cdot \phi} \tag{11}$$

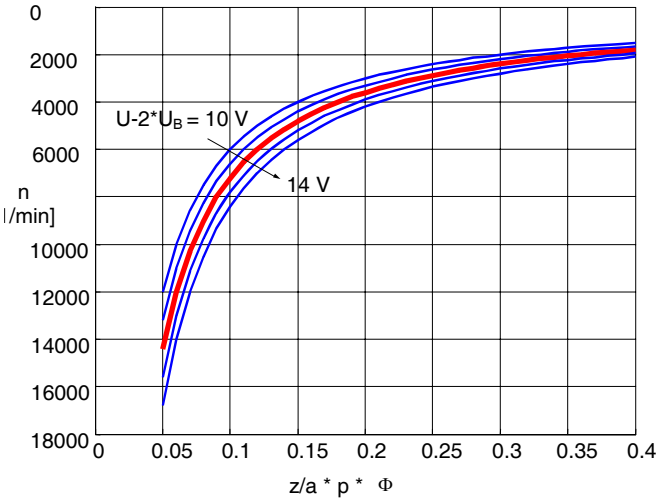

Fig. 7. Speed characteristic with voltage drop $U\text{-}2U_B$ as parameter ranging from 10… 14V.

Now we have all graphs, which will allow us to design the small DC motor. The design of a motor with a maximum speed of approximately 2000 1/min, a desired rated torque of M_r=0,15 Nm for a board-net voltage of U=14V can be performed. First we determine in Fig. 7 for the speed of 2000 1/min at the desired parameter $U\text{-}2U_B$=12V the maximum flux value $z/a \cdot p \cdot \phi \approx 0,35Vs$. The geometrical dimensions of the motor are now roughly determined by the flux value because the permanent magnets have to generate this flux. The manufacturers of the pole-magnets provide the geometrical dimensions. We now choose the operating point of M_r=0,15 Nm in Fig. 5 and can determine with Fig. 6 the rated current of I_r=3,5A. The short-circuit current can be estimated from this graph as well, respectively the short-circuit torque can be taken from Fig. 5.

The current values have to be checked if they are thermally allowed. If they are too high, the $z/a \cdot p \cdot \phi$ value has to be corrected to obtain permitted values for the rated current respectively torque. However, to optimise the motor, further iterations regarding the winding resistance, optimum torque respectively the maximum efficiency have to be performed. The extension of this approach is not difficult, but will not be discussed here. For further information the reader is referred to reference [2]. In this approach it is obvious that an ideal model of the motor is assumed. For example, the actual air-gap field distribution due to the armature current is not considered and in addition only the static motor behaviour was considered. By using a finite element model of the motor it is possible to evaluate the motor's behaviour in more detail. Models to simulate the dynamic behaviour of the machine are possible as well. In the following section an efficient modelling with the finite element method is discussed.

III. Finite Element Motor Models

To build up a FEM model, in a pre-process the device's geometrical shape is approximated by finite elements. In two-dimensional models the standard elements are commonly triangles and in the three-dimensional case tetrahedron elements can be used. This shape of the finite elements is very flexible and capable to approximate very well even complicated geometrical shapes (Fig. 8). For the following approach, it can be assumed, that one results of the finite element simulation the air-gap flux distribution $\phi = f(I,\theta)$ is. I is the armature current and θ the angular position in the air-gap.

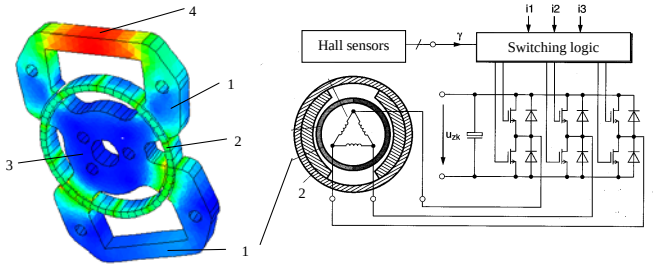

1 stator
2 permanent magnet system
3 rotor
4 winding

Fig. 8. Left: Magnetic field solution of a small motor and right: Principle of a brushless motor with power electronic circuit.

Outgoing from the dynamic form of the voltage equation obtained from Fig. 4 and neglecting the brush's voltage drop U_B because we consider now an ideal power electronic, which commutes the currents in the m winding phases of a brushless motor yields:

$$U = R_A I + \frac{\partial}{\partial t}\phi \tag{12}$$

Since $\phi = f(I,\theta)$ it can be written:

$$U = R_A I + (\partial_\theta \phi)\omega + (\partial_I \phi)\frac{\partial}{\partial t} I \tag{13}$$

The angular speed of the motor is $\omega = \frac{\partial}{\partial t}\theta$. The multiplication with the current I delivers the energy balance:

$$UI = R_A I^2 + (\partial_\theta \phi)\omega I + \frac{\partial}{\partial t}\psi \tag{14}$$

The term $\frac{\partial}{\partial t}\psi$ represents the time induced voltage drop due to the time dependency of the flux

$$\psi(I) = \int_0^I L(I) I \cdot dI \quad \text{with} \quad L(I) = \partial_I \phi \tag{15}$$

and $(\partial_\theta \phi)\omega I$ is the rotationally induced voltage. However, it must be noted, that $L(I) = \partial_I \phi$ is a non-linear inductance. By evaluating eq.(14) the following terms can be identified:
UI… the total electrical input power,
RI^2… the Joule losses of the winding,
$(\partial_\theta \phi)\omega I$ … the mechanical power of the system and
$\frac{\partial}{\partial t}\psi(I)$… represents the variation of the magnetic field energy in time. Averaging in time and multiplying by the motor's number of poles *2p* and the number of phases *m* the inner mechanical power can be distinguished in the shaft power $M\omega$ and the power consumed by the iron losses of the magnetic circuit Q_{iron}:

$$2pm\frac{\omega}{\pi / p}\int_0^{\pi/p}(\partial_\theta \phi)I \cdot d\theta = M\omega + Q_{iron} \qquad (16)$$

Other losses e.g. friction etc. can be considered at the right-hand side of eq.(16) as well.

The core losses can be distinguished in an eddy current and a hysteresis component. They can be expressed by:

$$Q_{iron}(I,\omega) = \underbrace{C_1(I)\omega}_{\text{hysteresis losses}} + \underbrace{C_2(I)\omega^2}_{\text{eddy current losses}} \quad . \qquad (17)$$

The frequency independent constants are determined by:

$$C_1(I) = \int_{stator}\left\{\int_0^{2\pi} h\partial_\theta b(\theta, I)d\theta\right\}$$
$$C_2(I) = \int_{stator}\left\{\frac{C_{eddy}}{2\pi}\int_0^{2\pi}\left|\partial_\theta b(\theta, I)\right|^2 d\theta\right\} \qquad (18)$$

The flux distribution $\phi = f(I,\theta)$ and the constants in eq.(18) depend on $b(\theta, I)$ and $\partial_\theta b(\theta, I)$. They can be computed in beforehand for a particular motor geometry by post-processing an appropriate series of 2D-FEM models. With this, the dynamic behaviour of the motor can be simulated. The motor's behaviour for arbitrary wave shapes of the current can be computed as well by applying a time-step scheme. With this, the control and the detailed power electronic circuit can be included in the model as well.

Figure 9 shows the results of a simulation of a small 3-phase brushless motor. Here the voltages appearing in the eq.(13) are plotted versus the rotor angle θ. In Fig. 10 the corresponding Torque is plotted.

IV. Conclusions

Numerical simulation is a powerful assistant in the field of small motor design. Decisively for a successful design is often the appropriate choice of motor model or the combination of different approaches to consider all relevant phenomena's. It is not compelling to solve the design task with only one flexible but complex tool. In many cases of practical relevance a combination of highly specialized simulation tools leads to qualified results. This is in particular true, when specialised motor designs with difficult specifications e.g. for automotive applications are aimed at.
In this paper the authors illustrate the design of small permanent magnet excited motors. The overall dimensions are determined by an analytical approach. The optimisation of the motor, subject to particular objectives can be performed by a numerical finite element model, which delivers the required and very accurate magnetic quantities.

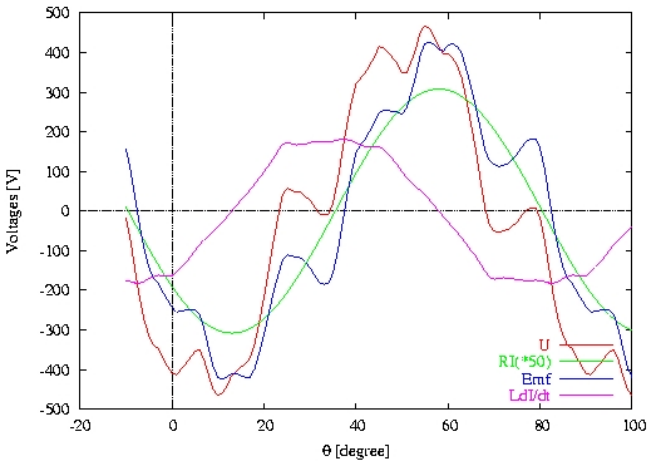

Fig. 9. Supply voltage, resistive voltage drop, induced voltage and self-inductance voltage versus the rotor position angle of a 3-phase brushless DC motor (compare also eq.(13) and Fig.4).

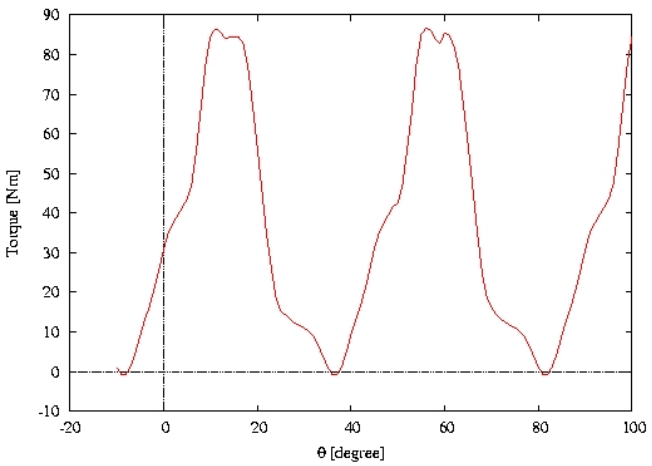

Fig. 10. Torque versus rotor angle θ.

References

[1] W.H. Yeadon; A.W. Yeadon, *Handbook of small electric motors*, McGraw-Hill, 2001.

[2] Mohr, A., *Kleinmotoren mit Permanentmagneterregung*, BOSCH, 1987.

[3] Hameyer, K. et al., *Numerical modelling and design of electrical machines and devices*, WIT Press, 1999.

[4] Miller, T.J.E., Brushles permanent magnet and reluctance motor drives, Clarendon Press, Oxford, 1989.